LBL-27477
Preprint

Lawrence Berkeley Laboratory
UNIVERSITY OF CALIFORNIA

Submitted to Physical Review Letters

Subthreshold Anti-Proton, K^-,K^+, and Energetic Pion Production in Relativistic Nucleus-Nucleus Collisions

A. Shor, E.F. Barasch, J.B. Carroll, T. Hallman, G. Igo,
G. Kalnins, P. Kirk, G.F. Krebs, P. Lindstrom, M.A. McMahan,
V. Perez-Mendez, S. Trentalange, F.J. Urban, and Z.F. Wang

August 1989

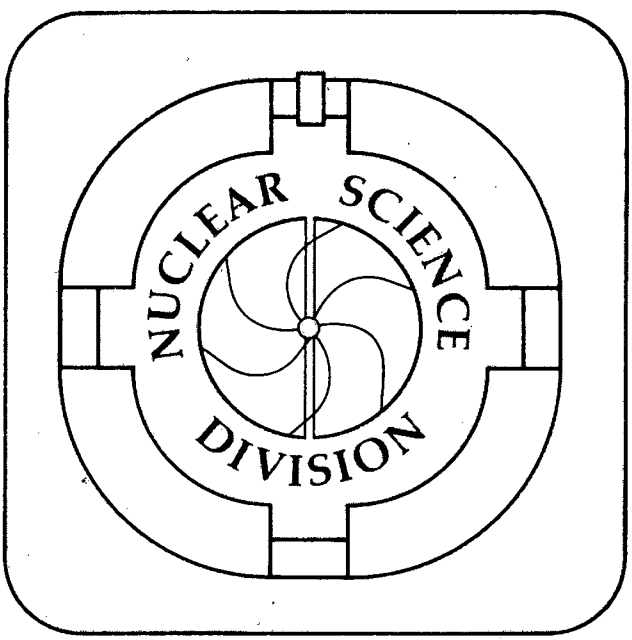

Prepared for the U.S. Department of Energy under Contract Number DE-AC03-76SF00098.

Subthreshold Anti-Proton, K^-, K^+, and Energetic Pion Production In Relativistic Nucleus-Nucleus Collisions

A. Shor[1,2], E.F. Barasch[3], J.B. Carroll[4], T. Hallman[5], G. Igo[4], G. Kalnins[1], P. Kirk[6], G.F. Krebs[1], P. Lindstrom[1], M.A. McMahan[1], V. Perez-Mendez[1], S. Trentalange[5], F.J. Urban[7], and Z.F. Wang[6]

1. Lawrence Berkeley Laboratory, Berkeley, CA 94720

2. Weizmann Institute of Science, Rehovot 76100, Israel

3. Texas A&M University, College Station, Texas 77843

4. University of California, Los Angeles, CA 90024

5. Johns Hopkins University, Baltimore, MD 21218

6. Louisiana State University, Baton Rouge, LA 70803

7. G.S.I , D-6100 Darmstadt 11, Fed. Rep. Germany

Abstract

We present a measurement of anti-proton, kaon, and energetic pion production at 0^o for the reactions ^{28}Si+^{28}Si at 2.0 GeV/nucleon ($E_{available}$/A=820 MeV) and 1.65 GeV/nucleon ($E_{available}$/A=700 MeV), and for ^{20}Ne+NaF at 2.0 GeV/nucleon. For a given reaction, the particle yields exhibit a scaling behavior independent of particle species.

PACS numbers 25.70Np

The study of subthreshold particle production in relativistic nucleus-nucleus collisions, especially at values of E/A much lower than the threshold for production of the particle in p-p collisions, provides an interesting probe of collective phenomena at large nuclear densities and temperatures. Since conventional sources of particle production hardly contribute at subthreshold energies, subtle phenomena at large nuclear densities may become evident by an enhancement of these particle yields over the expected rates. Subthreshold pion production has been observed in light ion collisions at bombarding energies as low as 25 MeV/nucleon[1,2], and in collisions of heavy nuclei at bombarding energies down to 138 MeV/nucleon.[3,4] Subthreshold K^- production has been detected for collisions of light ions at bombarding energies ranging from 2.0 GeV/nucleon down to 1.0 GeV/nucleon.[5] At bombarding energies of 1-2 GeV/nucleon, nuclear densities are expected to approach 3-4 times normal nuclear matter densities,[6] which may be sufficient for the creation of exotic nuclear states (such as Lee-Wick matter,[7] pion condensation,[8] etc.) predicted to occur at large nuclear densities.

Carroll et al.[9] reported the first observation of anti-proton production with nuclear beams, in the reaction ^{28}Si + ^{28}Si at 2.1 GeV/nucleon. The $\overline{p}$ yield observed in this measurement is more than 3 orders of magnitude larger than expected on the basis of calculations[10] that take into account the internal nuclear momentum of the projectile and target nucleons. This same set of calculations is able to reproduce experimental data on subthreshold anti-proton production in p+Cu collisions[11], where for bombarding energies ranging from 6 GeV down to 2.9 GeV, the $\overline{p}$ yields drop by 6 orders of magnitude. The basic ingredient in this calculation is a parameterization for the internal nuclear momentum based on data from electron scattering[12], and backward proton production.[13] Subthreshold anti-proton production has also been observed in Dubna[14], although at a

significantly higher bombarding energy, for the reaction ^{12}C + ^{63}Cu at 3.65 GeV/nucleon ($E_{available}$/A=1350 MeV).

We report on a recent experiment in which we measured $\overline{p}$, K^-, K^+, and π^- production at 0^o in the reaction ^{28}Si + ^{28}Si at 2.0 GeV/nucleon ($E_{available}$/A=820 MeV), and $\overline{p}$, K^-, and π^- production for ^{28}Si + ^{28}Si at 1.65 GeV/nucleon ($E_{available}$/A=700 MeV), and for ^{20}Ne + NaF at 2.0 GeV/nucleon. The measurements were made at the Lawrence Berkeley Laboratory BEVALAC accelerator on a beam line designed specifically for this measurement. Secondary particles produced at the production target were guided along a spectrometer consisting of two magnetic bends and focusing elements. Detector stations at beam focii included scintillation counters for TOF and beam definition, aerogel Cerenkov ($\beta_{thresh} \sim 0.98c$) and focusing liquid Cerenkov ($\beta_{thresh} \sim 0.9c$) counters, and at the end station a lead glass array to measure total deposited energy. The spectrometer, discussed in reference 9, will be described elsewhere.[15] The beam intensity was at 5×10^9 ions/spill, with a production target of thickness corresponding to 50 % interaction length for ion-ion collisions.

The data analysis included cuts on the scintillation counter pulse heights to define the beam and reduce effects due to pile-up, as well as cuts on the Cerenkov counters to highlight the kaon and anti-proton signals. The data is normalized to previously measured pion cross sections, [16] and corrected for absorption of the secondaries (including $\overline{p}$ annihilation)[17] in the prodution target and detectors, and for the decay of pions and kaons. The ion energies quoted are the mean energies after taking into account the dE/dX of the ions in the production target.

Figure 1 illustrates the quality of the data for secondaries produced at 1.9 GeV/c and 0^o in the reaction ^{28}Si +^{28}Si at 2.0 GeV/nucleon. The left hand side of figure 1 shows

the Time of Flight (TOF) measurements over the 7 meters flight path between detector station 1 and 2 (relative to pions). At top left, the TOF spectrum for negative particles not vetoed by the aerogel Cerenkov counters is shown. A clear distinction between the π^- and K^- peaks is seen, and even the anti-proton peak appears above the background. (Note that the aerogel Cerenkov counters together were only 99.9% efficient to pions.) The middle left plot shows the TOF for events which also did not trigger the liquid Cerenkov counters. A distinct signal containing 50 anti-protons is seen. Out of 2×10^8 events, only 2 pions survived the Cerenkov vetoes, with no other events (aside from the $\overline{p}$ events) seen over the 50 nanosecond TOF window. This data is taken from two separate runs, with a 50 % and a 25 % ion-ion interaction length target respectively. The ratios of π^-, K^-, and $\overline{p}$ were consistent for these targets. The bottom left figure shows the TOF distribution when the line was tuned for positive secondaries at the same momentum. Peaks corresponding to π^+, K^+, and protons appear at the same postion in TOF as their negatively charged counterparts. The plots on the right side of figure 1 show the total response of the lead glass array, in units of equivalent electromagnetic energy, for pion, anti-proton, and proton events. These distributions of pulse heights differ significantly, with the anti-proton events depositing more equivalent electromagnetic energy than the proton events and the pion events at the same momentum. This rules out the possibility that the $\overline{p}$ events are H^- ions.

Figure 2 shows the invariant cross sections for $\overline{p}$, K^-, K^+, and π^- production as a function of the particle kinetic energy in the nucleus-nucleus center of mass ($KE_{c.m.}$), for the reaction $^{28}Si + ^{28}Si$ at 2.0 GeV/nucleon. Also added are several data points from previous π^- and K^- measurements.[18] The π^- and K^- distributions appear to be exponential, i.e. $Ed^3\sigma/d\vec{P}^3 \sim exp(-KE_{c.m.}/E_o)$, with the slope parameter $E_o = 108 \pm 7$

MeV for the π^-, and a similar value of $E_o = 103 \pm 7$ MeV for the K^-. The π^- slope parameter, measured here at 0^o, is similar to the value of $102 \pm 5 MeV$ measured for pions at 90^o in the c.m. for Ne+NaF at 2.1 GeV/nucleon[19]. Our K^+ spectrum, with E_o of 240 ± 92 MeV, is much flatter than the value of 140 MeV reported by Schnetzer et al.[20] for Ne+NaF$\rightarrow K^+$ at finite laboratory angles, and may reflect contribution from associated production at small angles. Lastly, our $\overline{p}$ spectrum appears to have a dip at $KE_{c.m.}=0$, although the statistical uncertainties do not make it possible to rule out an exponential falloff. The $\overline{p}$ slope parameter obtained by fitting the two higher energy data points yield a value for E_o of 120 ± 50 MeV, similar to E_o for the π^- and K^-, whereas a value for E_o of 210 ± 98 MeV is obtained when fitting all three $\overline{p}$ data points. A dip in the $\overline{p}$ spectrum at low $\overline{p}$ c.m. velocities can be expected if the anti-protons are produced in central collisions and where a large number of nucleons exist at mid-rapidity, since $\overline{p}$-p annihilation cross sectionas are large ($\sigma \sim 200$ mb) at low relative velocities.[21]

We mention a very interesting feature appearing in figure 2. At a fixed value of $KE_{c.m.}$, the difference in the invariant cross section between π^- and K^- production is almost identical to the difference between the K^- and $\overline{p}$ production. The threshold excitational energy required for particle production in p-p collisions, denoted by E_{thresh}, is equal to m_π for pion production, $2\times$ m_K for K^- production, and $2\times$ m_p for anti-proton production. It is an interesting coincidence that the differences in E_{thresh} between pions and K^-, i.e. $(2 \times m_K - m_\pi) = 848 MeV$, is very close in absolute value to the difference in E_{thresh} between K^- and $\overline{p}$ production , i.e $(2 \times m_p - 2 \times m_K) = 884 MeV$. This feature leads us to the speculation that particle production for this reaction scales with the excitation energy required, independent of particle type.

The above feature is exploited in figure 3, which contains the same invariant cross

sections for π^-, K^-, K^+, and $\bar{p}$ as in figure 2, but plotted as a function of the variable E^* = E_{thresh} + $KE_{c.m.}$ (note that for K^+, E_{thresh} = (m_Λ-m_N) + m_K). The particle yields exhibit a scaling in the variable E^* which appears not to be dependent on the particle type. Slight deviations from this scaling are noticeable, although the general trends follow this scaling over 9 orders of magnitude. The deviations from scaling may be due to the difference in final state interactions at the later stages of the collision process for the different particle types.[22] Figures 4 and 5 show the invariant cross sections for π^-, K^-, and $\bar{p}$ production for the reactions ^{28}Si + ^{28} at 1.65 GeV/nucleon and for ^{20}Ne + NaF at 2.0 GeV/nucleon, respectively, also as a function of the variable E^*. The scaling behavior is also demonstrated for each of these reactions.

The universal scaling may be parameterized by an exponential function, i.e. $Ed^3\sigma/d\vec{P}^3 = K_s exp(-E^*/E_s)$, where the variables E_s and K_s depend on the bombarding energy and the size of the colliding system. Since there are deviations from the scaling behavior, a least χ^2 fit of all the data points would be dominated by the π^- and K^- data which contain the smallest statistical error bars, and would miss the $\bar{p}$ data points by a considerable amount. We have therefore chosen to estimate the value of E_s for the reactions shown in figures 3-5 by connecting only the data points for pions at $KE_{c.m.}$= 270 MeV with that for $\bar{p}$ at $KE_{c.m.}$= 55 MeV. The solid curves shown in figures 3-5 reflect a value of $E_s = 87MeV$ for Si+Si at 2 GeV/n, $E_s = 80MeV$ for Si+Si at 1.65 GeV/n, and $E_s = 86MeV$ for Ne+NaF at 2 GeV/n.

The scaling behavior observed for particle production in nucleus-nucleus collisions suggest a common production mechanism independent of particle type. This is an important generalization since it would disfavor a mechanism peculiar to one particular particle species, such as the strangeness exchange mechanism ($Y\pi \rightarrow K^-N$) to explain subthreshold

K^- production. Since most of the data in figures 3-5 lie beyond the energies accessible to individual N-N collisions (i.e., for values of $E^* > E_{available}/A$), a collective mechanism for the production of heavy and energetic particles in relativistic nuclear collisions is inferred. An attempt to find scaling for particle production in nucleus-nucleus collisions has also been reported by Baldin et al.[23] The scaling we observe is similar in nature to that studied by Hagedorn[24] in high energy p-p collisions, with the distinction that the scaling reported here is mostly for products that require more energy than is available in the average N-N collision.

We would like to thank the engineering and operations staff of the BEVALAC for their support during the experimental program. The BEVALAC performance during this experiment was truly outstanding, with a record Silicon intensity over an extended period of time. We thank H. Stroeher for assistance in setting up the experiment. This work was supported by the Director, Office of Energy Research, Office of High Energy and Nuclear Physics, Nuclear Physics Division of the U.S. Department of Energy under contracts DE-AC03-76S00098, DE-FG03-88ER40424, DE- FG0288ER40413, DE-FG05-88ER40445, and DE-AC02-76ER03274.

References

1. W. Benenson et al., Phys.Rev.Lett.43,683 (1979)
2. G.R. Young et al., Phys.Rev.C33, 742(1986).
3. G.F. Krebs et al., Phys.Lett.171B, 37 (1986).
4. J. Miller et al., Phys.Rev.Lett.58, 2408 (1987).
5. J.B. Carroll et al., Nucl.Phys. A488, 203c (1988).
6. J. Cugnon, T. Mizutani, and J. Vandermeulen, Nucl.Phys. A352, 505 (1981).
7. T.D. Lee, Rev.Mod.Phys. 47, 267 (1975).
8. A.B. Migdal, Rev.Mod.Phys. 50, (1978).
9. J.B. Carroll et al., Phys.Rev.Lett. 62, 1829 (1989).
10. A. Shor, V. Perez-Mendez, and K. Ganezer, LBL-17067 (1984).
11. D.E. Dorfan et al., Phys.Rev.Lett.14, 995(1965).
12. E.J. Moniz et al., Phys.Rev.Lett.26, 445(1971).
13. J.V. Geaga et al., Phys.Rev.Lett.45, 1993(1980).
14. A.A. Baldin et al., JETP Lett. 47, 137 (1988).
15. In preparation and to be published.
16. E.F. Barasch, Thesis, University of California, Davis, 1986.
17. K. Nakamura et al., Phys.Rev.Lett. 52, 731 (1984). and R.J. Abrams et al., Phys.Rev. D4, 3235 (1971).
18. E.F. Barasch et al., Phys.Lett. 161B, 265 (1985).

19. S. Nagamiya et al., Phys.Rev. $C24$, 971 (1981).

20. S. Schnetzer et al., Phys.Rev.Lett. 49, 989 (1982).

21. Particle Data Book, Phys.Lett. $B204$, 127 (1988).

22. S. Nagamiya, Phys.Rev.Lett. 49, 1383 (1982).

23. A.A. Baldin et al., 'Proc.Int.Conf. on Extreme States of Nuclear Systems,' Dresden zfk-430, 1980, p.1 and A.A. Baldin et al., Internal Dubna Report D2-82-568.

24. R. Hagedorn, CERN report 71-12 (1971).

Figure Captions

Figure 1.^{28}Si + ^{28}Si $\rightarrow$ secondaries at P=1.9 GeV/c and 0°. Spectra on left show time of flight for negatives with aerogel Cenrekov veto (top), aerogel and liquid cerenkov veto (middle), and for positives (bottom). Spectra on right show lead glass response for pions (top), anti-protons (middle), and for protons (bottom).

Figure 2.Invariant cross sections for π^-, K^+, K^-, and $\overline{p}$ production at 0° for the reaction ^{28}Si + ^{28}Si at 2.0 GeV/nucleon, plotted as a function of particle kinetic energy in the nucleus-nucleus center of mass frame ($KE_{c.m.}$).

Figure 3.Invariant cross sections for π^-, K^+, K^-, and $\overline{p}$ production at 0° for the reaction ^{28}Si + ^{28}Si at 2.0 GeV/nucleon ($E_{available}/A = 820MeV$) plotted as a function of the scaling variable $E^* = E_{thresh} + KE_{c.m.}$ (same data as in figure 2).

Figure 4.^{28}Si + ^{28}Si at 1.65 GeV/nucleon ($E_{available}/A = 700MeV$).

Figure 5.^{20}Ne+NaF at 2.0 GeV/nucleon ($E_{available}/A = 820MeV$)

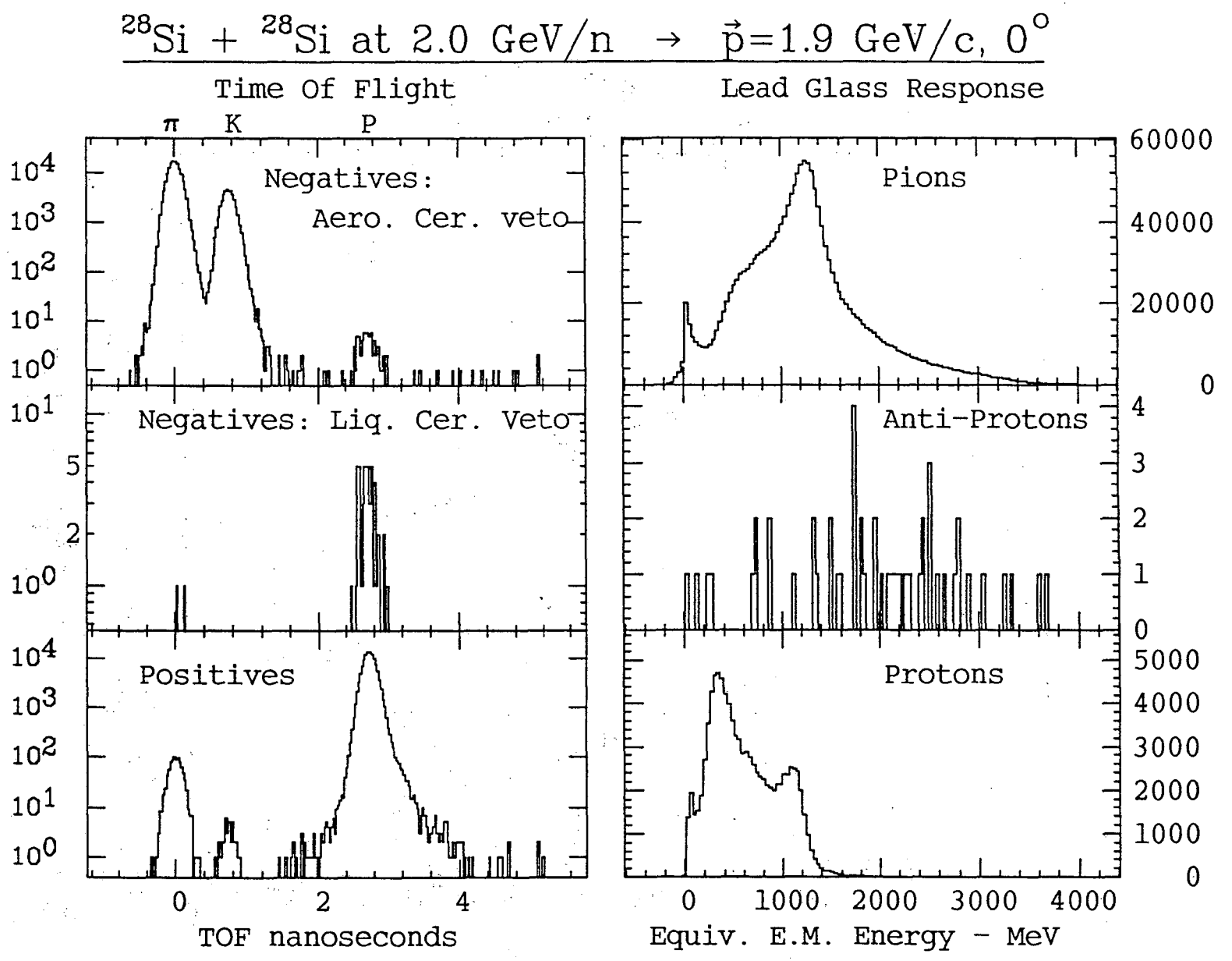
$^{28}Si + {}^{28}Si$ at 2.0 GeV/n → $\vec{p}$=1.9 GeV/c, 0°
Time Of Flight
Lead Glass Response
π
K
P
Negatives:
Aero. Cer. veto
Negatives: Liq. Cer. Veto
Positives
Pions
Anti-Protons
Protons
TOF nanoseconds
Equiv. E.M. Energy - MeV

Figure 1

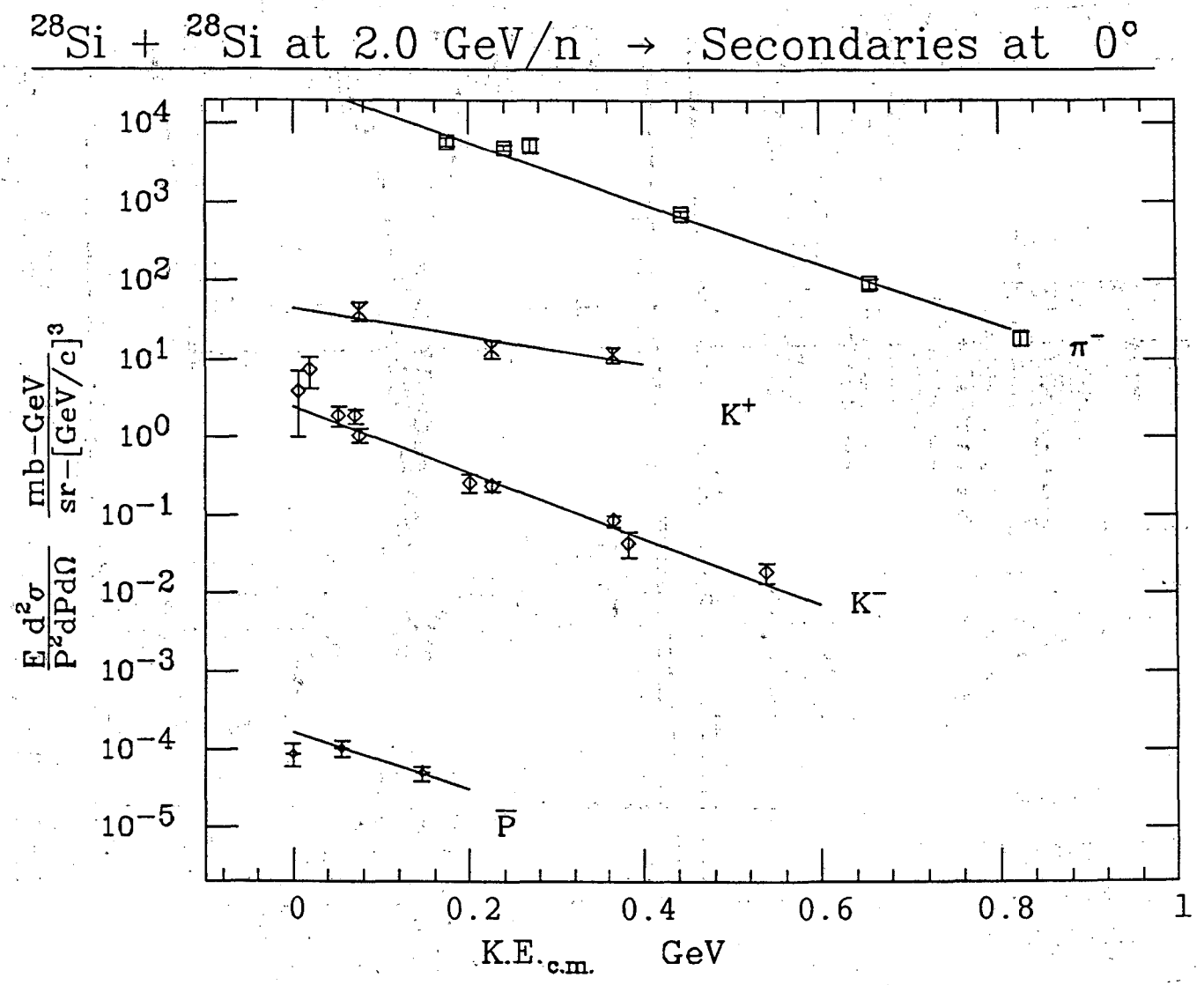
$^{28}Si + {}^{28}Si$ at 2.0 GeV/n → Secondaries at 0°
$\frac{E\,d^2\sigma}{P^2dPd\Omega}\ \frac{mb-GeV}{sr-[GeV/c]^3}$
10^4
10^3
10^2
10^1
10^0
10^{-1}
10^{-2}
10^{-3}
10^{-4}
10^{-5}
π^-
K^+
K^-
$\bar{P}$
0
0.2
0.4
0.6
0.8
1
K.E.$_{c.m.}$ GeV

Figure 2

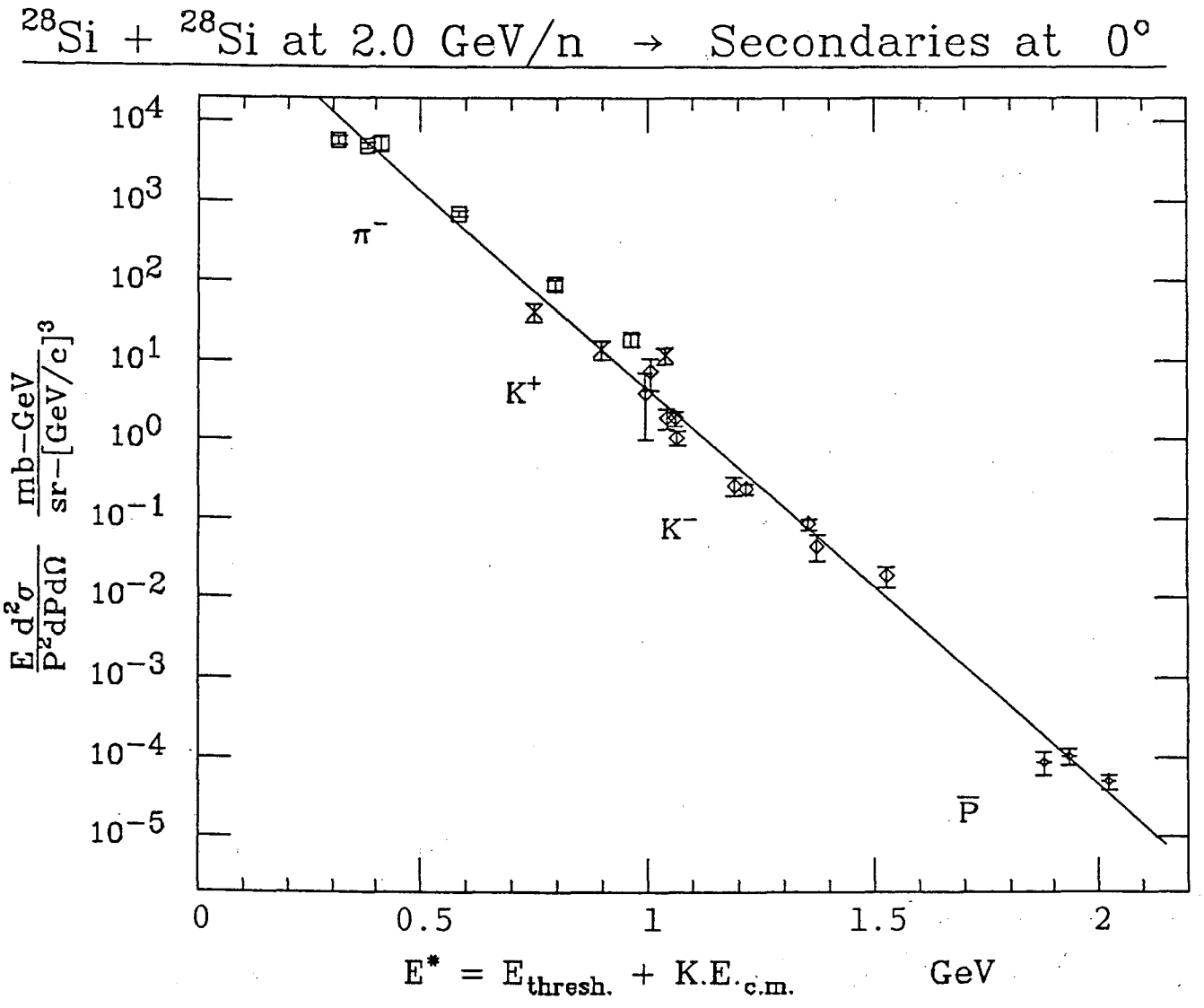
^{28}Si + ^{28}Si at 2.0 GeV/n → Secondaries at 0°
$\frac{E}{P^2}\frac{d^2\sigma}{dPd\Omega}$ $\frac{mb-GeV}{sr-[GeV/c]^3}$
10^4
10^3
10^2
10^1
10^0
10^{-1}
10^{-2}
10^{-3}
10^{-4}
10^{-5}
π^-
K^+
K^-
$\bar{P}$
0
0.5
1
1.5
2
$E^* = E_{thresh.} + K.E._{c.m.}$
GeV

Figure 3

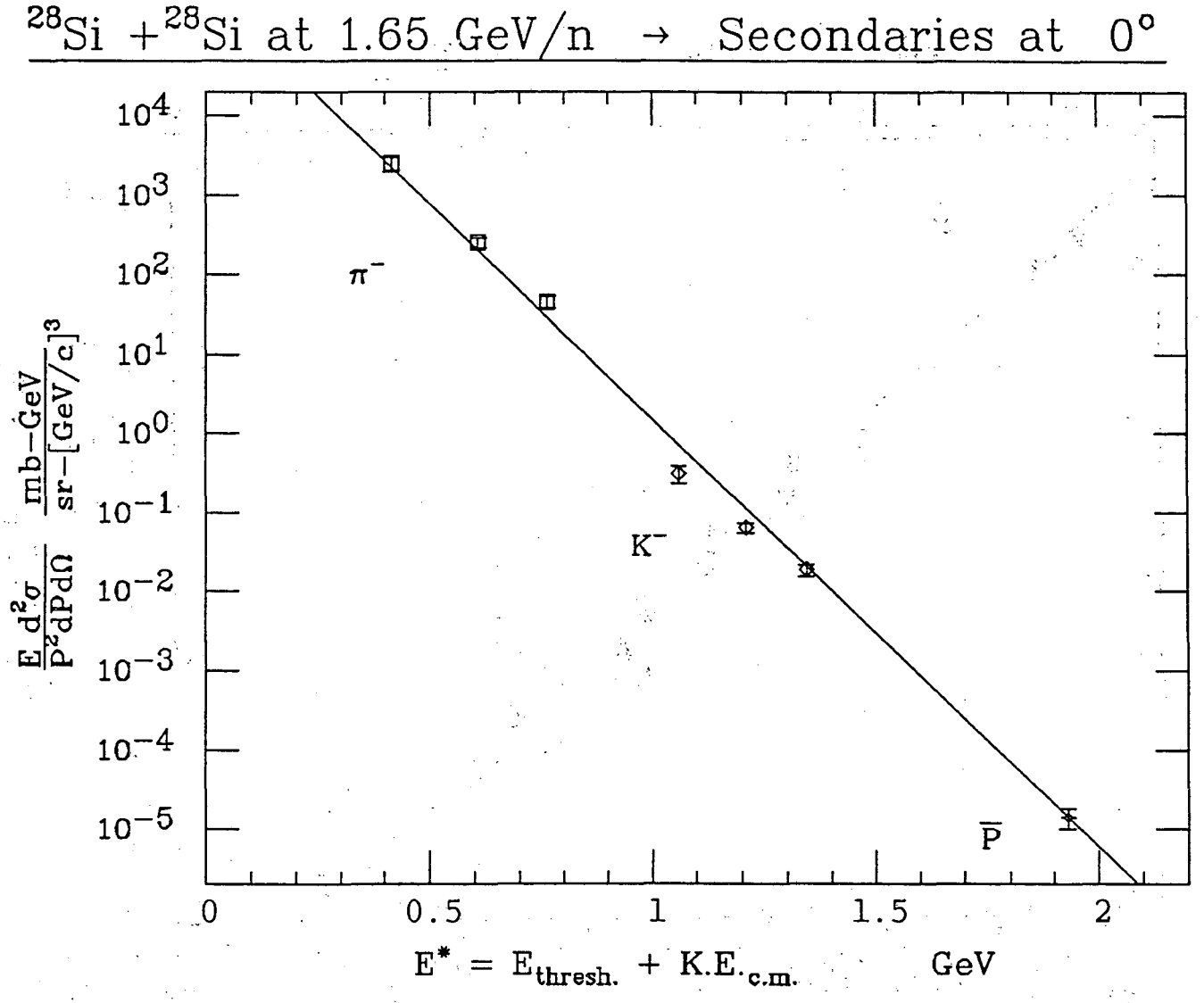
$^{28}Si + ^{28}Si$ at 1.65 GeV/n → Secondaries at 0°
$\frac{E\,d^2\sigma}{P^2dPd\Omega}$ $\frac{mb-GeV}{sr-[GeV/c]^3}$
10^4
10^3
10^2
10^1
10^0
10^{-1}
10^{-2}
10^{-3}
10^{-4}
10^{-5}
π^-
K^-
$\overline{P}$
0
0.5
1
1.5
2
$E^* = E_{thresh.} + K.E._{c.m.}$ GeV

Figure 4

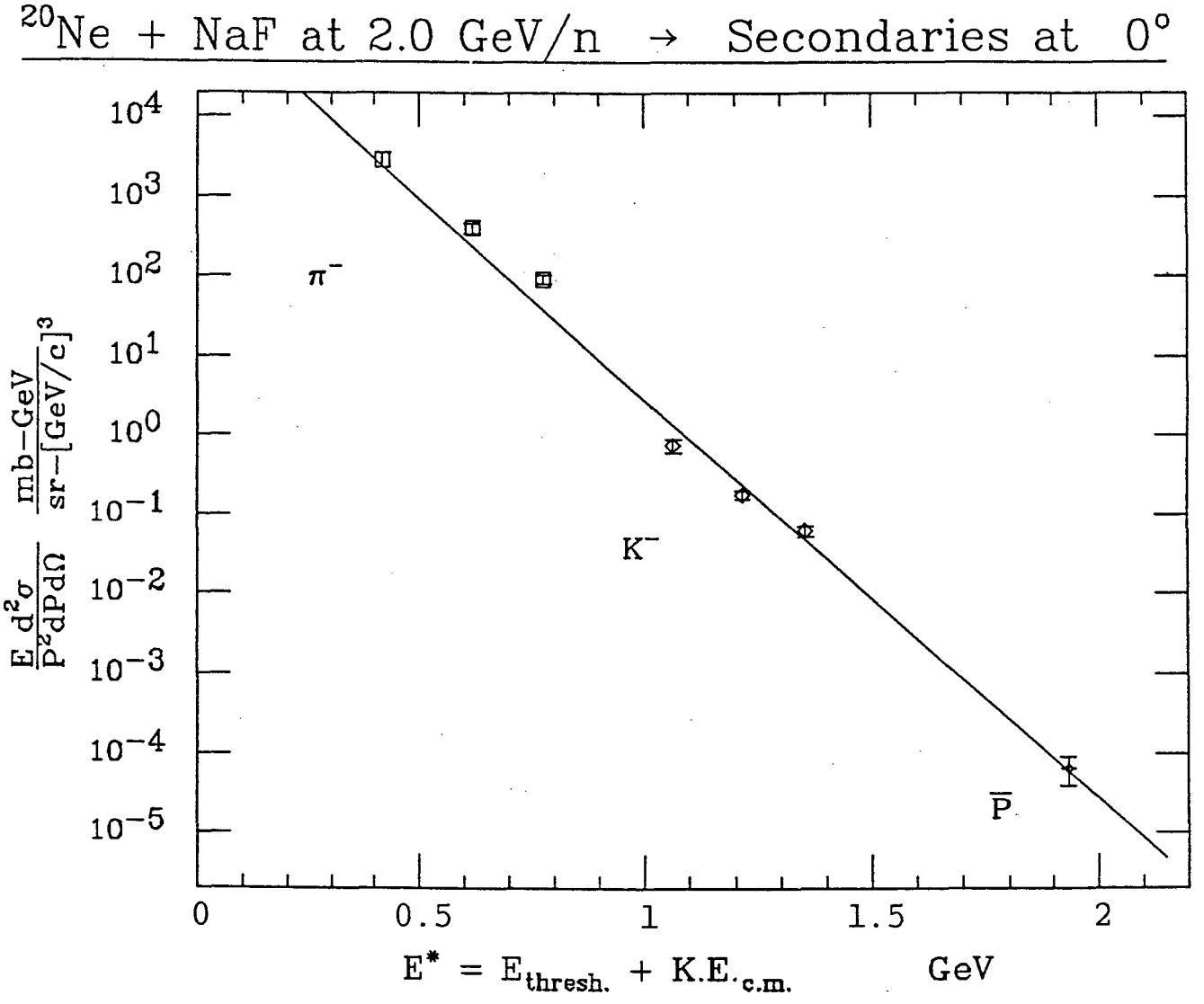
^{20}Ne + NaF at 2.0 GeV/n → Secondaries at 0°
$\frac{E\,d^2\sigma}{P^2 dP d\Omega}\ \frac{mb-GeV}{sr-[GeV/c]^3}$
10^4
10^3
10^2
10^1
10^0
10^{-1}
10^{-2}
10^{-3}
10^{-4}
10^{-5}
π^-
K^-
$\bar{P}$
0
0.5
1
1.5
2
$E^* = E_{thresh.} + K.E._{c.m.}$ GeV

Figure 5

LAWRENCE BERKELEY LABORATORY
TECHNICAL INFORMATION DEPARTMENT
1 CYCLOTRON ROAD
BERKELEY, CALIFORNIA 94720